Int. J. Electrochem. Sci., 15 **(2020)** 12122 – 12135, doi: 10.20964/2020.12.76

International Journal of ELECTROCHEMICAL SCIENCE
www.electrochemsci.org

Direct Electrodeposition to Fabricate Vertically Aligned Reduced Graphene oxide–diphenylalanine Network for Highly Sensitive Amperometric Nitromethane Biosensors

Qunpeng Duan[1], *Lijie Wang*[1], *Shimin Wang*[1], *Kui Lu*[1,2,*]

[1] School of Material and Chemistry Engineering, Henan University of Engineering, Zhengzhou, 450007, PR China
[2] School of Chemical Engineering and Food Science, Zhengzhou Institute of Technology, Zhengzhou, 450044, PR China
[*]E-mail: luckyluke@haue.edu.cn (Kui Lu)

Received: 17 August 2020 / *Accepted:* 19 October 2020 / *Published:* 31 October 2020

In this paper, vertically aligned electrochemically reduced graphene oxide-diphenylalanine (VA-ErGO-FF) network was directly prepared at glassy carbon (GC) electrode's surface from graphene oxide-diphenylalanine (GO-FF) dispersions by using a pulsed electrodeposition technique. The electrochemical experiments and scanning electron microscopy revealed properties in VA-ErGO-FF network. Model molecule hemoglobin was further fastened onto VA-ErGO-FF network to construct electrochemical nitromethane (CH_3NO_2) amperometric biosensors. Electrochemical results revealed that hemoglobin in the VA-ErGO-FF network retained its bioactivity, showing two quasi-reversible redox peaks and high bioelectrocatalytic activity to CH_3NO_2. Biosensor indicated extensive linear response scope as 1.0×10^{-6} - 5.0×10^{-4} mol L^{-1} in optimum circumstances, corresponding to low detection limit as 5.0×10^{-7} mol L^{-1}. It had been found VA-ErGO-FF network is a promising platform with bright prospects in the application of electrochemical biosensor for extraordinary biocompatibility as well as favorable charge-transfer capability.

Keywords: vertically aligned, electrochemically reduced graphene oxide-diphenylalanine, hemoglobin, direct electron transfer, nitromethane

1. INTRODUCTION

Nitromethane (CH_3NO_2), an aliphatic nitro compound in simplest composition, has been extensively used as an energy source. Whereas, nitromethane also proves to be one of the most widespread pollutants [1]. Long-term contact with nitromethane may cause detrimental impacts to people's physical conditions, like blood dyscrasias, thyroid toxicity, peripheral neuropathy [2]. Hence, tremendous efforts have been carried out to the determination of CH_3NO_2, which include colorimetry

[3], solid-phase microextraction (SPME)-gas chromatography (GC)-high resolution mass spectrometry (HRMS) (SPME-GC-HRMS) [4], infrared spectroscopy [5], as well as fluorimetry [6]. Nevertheless, most of these methods suffer from inherent limitations, such as requiring considerable samples regardless of high sensitivity. By far, hemeproteins' direct electrochemistry covering hemoglobin (Hb) [7], horseradish peroxidase (HRP) [8], cytochrome c (cyt c) [9] has attracted considerable concerns. By expounding enzyme electron transfer during biological activity [10], it simultaneously constructs a useful solution for the construction of biosensor [11]. Because of its prominent characteristics, great stability and applicability for business uses, Hb has been extensively utilized in redox protein's direct electrochemistry as the model. Nevertheless, active site is buried deeply within the core of Hb and thus the electronic transfer of Hb to the electrode is blocked. Besides, with direct absorption on the surface of electrode, Hb usually loses its bioactivity [12, 13]. Therefore, it is hard to realize Hb's direct electron transfer (DET) for traditional electrode. Lots of materials can serve as the modifier for resolving this problem, like surfactant [14], conductive polymers [15], ionic liquids [16] as well as nanomaterials [17]. Up to now, some works have been carried out on the determination of CH_3NO_2 based on electrochemical biosensor [18-21]. Despite the progress made, it is feasible to introduce novel materials and approaches to DET-based biosensor design and CH_3NO_2 determination.

Graphene, a 2D sp^2-hybirdized carbon material, gains widespread concerns for great active surface area, good electrical conductivity, and outstanding electrochemical stability [22, 23]. Graphene-based electrochemical biosensors have been widely reported in the literature [24]. Whereas, graphene sheets are apt to generate 2D agglomerates because of intense π-π interaction, which significantly reduces its effectiveness. Hence, it is very important to design and construct vertically-aligned graphene sheets on substrate surface. Recently, a variety of approaches have been proposed, such as template [25], chemical vapor deposition (CVD) [26], and electrospray deposition [27]. Direct electrodeposition is more environmentally friendly for non-addition of toxic chemicals, cheap, and proper for high-purity deposit preparation [28-31]. More importantly, it exhibits better conducting than that prepared by other methods [32, 33]. Furthermore, due to its hydrophobicity, the practical application of graphene in electrochemical biosensor preparation still presents a great challenge. Therefore, it is necessary to introduce DNA [34], ionic liquids [35], peptides [36] and small molecular weight polymers [37] to form functional graphene nanocomposites.

In this work, we report that vertically-aligned electrochemically reduced graphene oxide-diphenylalanine (VA-ErGO-FF) network was prepared at glassy carbon (GC) electrode's surface directly in GO-FF dispersion with pulsed potentiostatic method (PPM). Model molecule hemoglobin was further fastened onto VA-ErGO-FF network to construct electrochemical nitromethane (CH_3NO_2) amperometric biosensors. Here, diphenylalanine (FF), which works as a modifier due to its biocompatibility, may further immobilize Hb on graphene-based films. Thorough studies had been performed to examine existing biosensors' electrochemical performance, Hb DET and CH_3NO_2 electrochemical measuring included. The research showed electrochemical biosensors demonstrated favorable electrochemical reactions to two stationary and approximately symmetric redox peaks of Hb, and exhibited superb electrocatalytic activity to CH_3NO_2. VA-ErGO-FF network is forecast to have bright availability in electrochemical biosensors.

2. EXPERIMENTAL

2.1. Apparatus and Reagents

UV-vis spectroscopy data were gathered with UV-2102 spectrophotometer developed by Chinese enterprise UNICO. Atomic force microscopy (AFM) analysis had been finished with Dimension FastScan AFM developed by German enterprise Bruker. Scanning electron microscopy (SEM) image was gathered by MERLIN's field emission scanning electron microscopic (FESEM) developed by German company Zeiss and Quonxe-250 scanning electron microscope developed by Czech enterprise FEI. Electrochemical tests including electrochemical impedance spectroscopy (EIS), cyclic voltammetry (CV), amperometric *i-t* curve were measured by CHI 650A electrochemical analyzer developed by Chinese enterprise CHI Instrumental. Traditional three-electrode system gained application, in which saturated calomel electrode (SCE) was reference electrode, platinum (Pt) wire electrode was auxiliary electrode, modified GCE (d = 3.0 mm) was working electrode.

High-purity flake graphite (325 meshes) was fabricated by XFNANO Materials Tech Co., Ltd in Nanjing, China. FF had been provided by Zhejiang Ontores Biotechnologies Co., Ltd. Remaining reagents like chitosan (Cs), Hb, CH_3NO_2, $K_4[Fe(CN)_6]$, $NaNO_3$, $KMnO_4$, H_2O_2, HCl, H_2SO_4 was fabricated by Aladdin Chemistry Co., Ltd in Shanghai. Phosphate buffer tablet came from Aldrich (Shanghai, China). As entire reagent had ensured grades, there was no need to have purification in practice. Solution preparation was made with doubly distilled water (DDW).

2.2. Preparation of GO and GO-FF

First, GO preparation was made with improved Hummer's approach from high-purity flake graphite [38]. Subsequently, it was rinsed in 5% HCl solution till the removal of SO_4^{2-} and DDW repeatedly till the removal of Cl^-. Eventually, moisture in solid product was eradicated after filtering and rinsing in acetone for three or four times, and GO would be obtained from lyophilized residue.

50 mg GO was dissolved with 10 mL DDW for sonication of 1 h, and 5 mg FF was added to the prepared GO dispersions and ultrasonicated for 30 min under ice-bath. The compound was continually stirred for response of 12h indoors. Following the centrifugation for half an hour, the black dispersion was cleaned by DDW for three times, and dried by lyophilizing for obtainment of GO-FF nanocomposites. It was easily dispersed with 0.2 mol L^{-1} pH 6.8 phosphate buffer (PB) solution by ultrasonication again.

2.3 Construction of the biosensor

Before application, bare GC electrode (d = 3 mm) gained successive polishment using 0.05 μm Al_2O_3 powder and cleaned by DDW in every procedure. Before the experiment, polished GC electrode was immersed with ethanol, DDW for 1 min for sonication, and dried by N_2 blowing. Rinsed GC electrode would be impregnated by GO-FF dispersions, and VA-ErGO-FF network modifed electrode (VA-ErGO-FF/GCE) was prepared from electrodeposition with PPM under stirring. Parameter setting

in pulse electrodeposition was: upper limit potential E_a, 0.1 V; lower limit potential E_a, -1.2 V; cathodic pulse duration t_c, 0.7 s; anodic pulse duration t_a, 0.3 s; experimental time t_{exp}, 150 s. By dropping 10 μL Cs-Hb solution, with 10 mg Hb dissolved in 1 mL 1 mg mL^{-1} Cs solutions, onto electrode surface, Cs-Hb/VA-ErGO-FF/GCE biosensor came into being. For comparison purposes, ErGO/GCE, Cs-Hb/GCE, Cs-Hb/ErGO/GCE, Cs/VA-ErGO-FF/GCE were also prepared with the same flow.

3. RESULTS AND DISCUSSION

3.1. Characteristics of GO and GO-FF

The morphologies of GO and GO-FF were examined by AFM. As can be seen, mean GO sheet thickness is around 1 nm in accordance with the cross-sectional profiles (Fig.1A), indicating the single layer of GO sheet. While mean GO-FF thickness ascended to around 3-5 nm (Fig.1B). Furthermore, there were numerous nanowires on GO sheet surface, suggesting successful immobilization of FF onto GO sheet surface.

UV-vis absorption data were gathered for comparing GO and GO-FF in absorption band changes (Fig.2A).

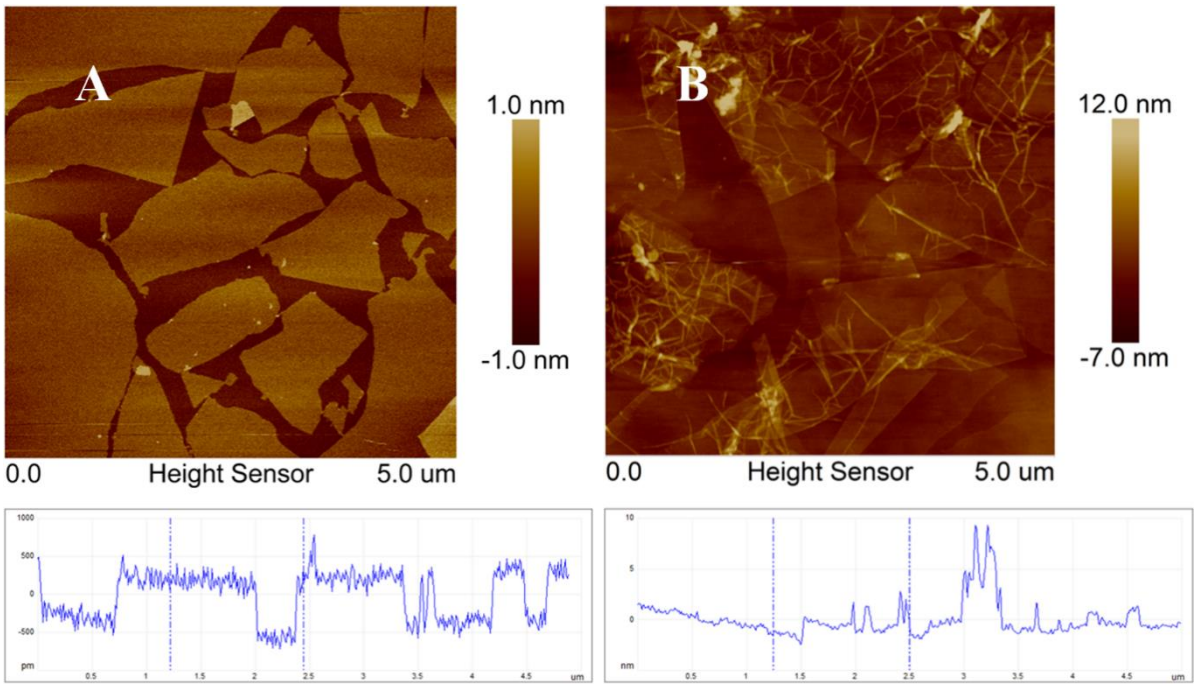

Figure 1. GO (A) and GO-FF (B) of AFM images in dilute aqueous dispersion of rinsed mica.

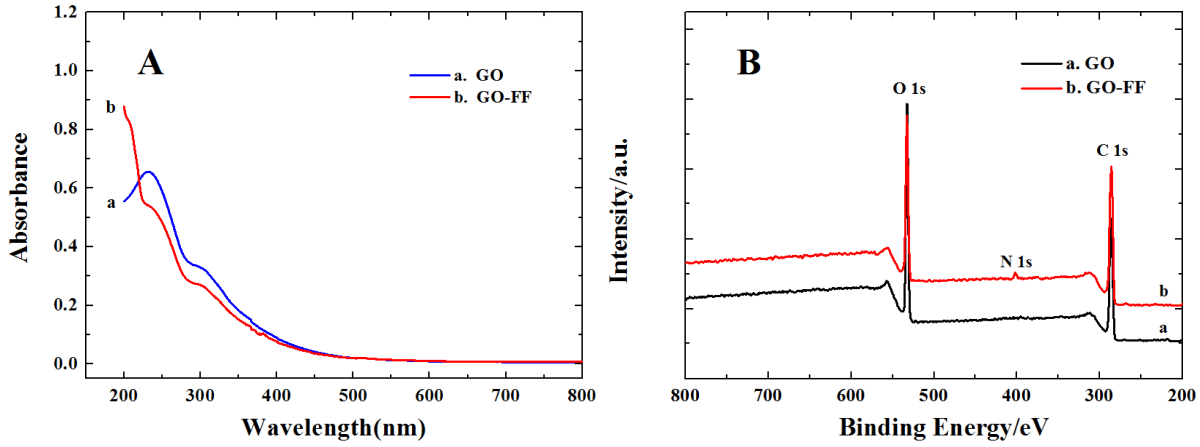

Figure 2. (A) GO (curve a), GO-FF (curve b) UV-visible absorption spectra; (B) GO (curve a), GO-FF (curve b) XPS survey spectra.

GO exhibited well-characterized absorption at 240 nm and 310 nm, while GO-FF remarkably dropped and then sharply increased at about 200 nm, implying the GO-FF bonding via π–π interaction [39]. And we found that GO-FF suspension remains stable even after one month of deposition, which favors to directly electrodeposit GO nanocomposites. Further, GO and GO-FF electronic structure and composition were determined by XPS analysis. There occurred a notable N1s peak from FF in GO-FF (Fig.2B), while no N signal was observed for GO, meaning the success of FF's chemical modification of FF for GO.

3.2. Characteristics of VA-ErGO-FF network modifed electrode

Literature [40, 41] posits the feasibility to have electrochemical reduction on GO nanocomposites in condition of E = -1.2 V *vs* SCE. Where -1.2 V *vs* SCE had been also applied in the electrochemical reduction on GO-FF nanocomposites. The FF ratio (FF:GO) and experimental time (t_{exp}) was evaluated with $[Fe(CN)_6]^{3-/4-}$ as redox probe. Fig.3A reveals how FF ratio affects electrochemical performance of VA-ErGO-FF modifed electrode. When the FF ratio was greater than 1:10, the response peak currents significantly decrease. Besides, no VA-ErGO-FF film had been found at GC electrode's surface after FF ratio was greater than 1:5. Hence, 1:10 as the optimal ratio was chosen. At the same time, the respose peak currents grow gradually with growing t_{exp}. But the VA-ErGO-FF film is easy to fall off. So t_{exp}=150 s was used for further studies.

Fig.3B displays cyclic voltammograms (CVs) in 1.0×10^{-3} mol L^{-1} $[Fe(CN)_6]^{3-/4-}$ redox couple (1:1) on bare GCE, VA-ErGO/GCE, VA-ErGO-FF/GCE surface in 0.1 mol L^{-1} KCl solutions. Unlike bare GCE, response peak currents (i_p) obviously grow as peak-to-peak separation (ΔE_p) declines on VA-ErGO/GCE. Moreover, no significant change of i_p and ΔE_p has been detected from VA-ErGO-FF/GCE. Results showed FF introduction did not significantly affect the conductivity of VA-ErGO film. Furthermore, SEM was used to characterize the nanostructure of VA-ErGO-FF (Fig.4). Individual sheet edge was differentiated by kinked (Fig. 4A), and interconnected network occurred at GC electrode surface. Interconnected network comprises VA-ErGO-FF nanosheets (Fig.4B), and provides greater

active surface for rapid electronic transport. It is highly beneficial for the electrochemical sensing applications.

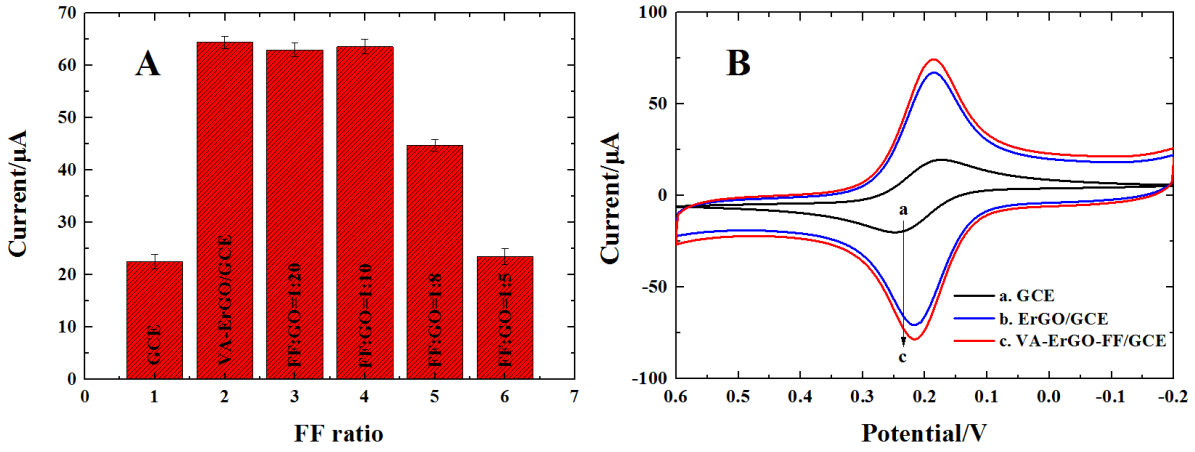

Figure 3. (A) Effect of FF ratio (FF:GO) on VA-ErGO-FF/GCE electrochemical performance; (B) Bare GCE (curve a), VA-ErGO/GCE (curve b), VA-ErGO-FF/GCE (curve c) CV in 1.0×10^{-3} mol L^{-1} $K_3[Fe(CN)_6]$ + 0.1 mol L^{-1} KCl solutions, v=0.050 V s^{-1}.

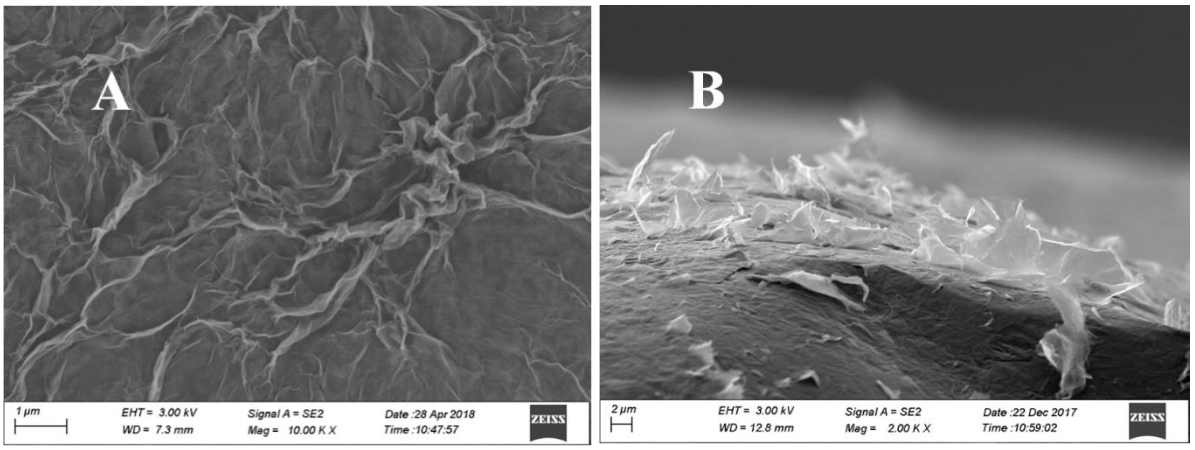

Figure 4. Top view SEM images (A) and cross-sectional SEM images (B) retrieved by VA-ErGO-FF/GCE.

3.3. Characteristics of Cs-Hb/VA-ErGO-FF modified electrode

For proving VA-ErGO-FF network's edge, model molecule Hb was fastened onto VA-ErGO-FF network. Electrochemical impedance spectroscopy (EIS) may offer information concerning electrode impedance change in modification. Fig.5 shows Nyquist plots for various electrodes of 5.0×10^{-3} mol L^{-1} $K_3[Fe(CN)_6]/K_4[Fe(CN)_6]$ (1:1) solution with 0.10 mol L^{-1} KCl. Equivalent circuit of Fig.5 was proposed to fit experimental value with model computed by ZSimpWin software. Electron transfer

resistance (R_{et}) of GCE was obtained as 85 Ω. On VA-ErGO/GCE and VA-ErGO-FF/GCE, R_{et} decreased to almost zero, indicating that VA-ErGO and VA-ErGO-FF nanostructure are very good conductive. When Cs-Hb/VA-ErGO-FF/GCE was applied, R_{et} increased to 642 Ω, suggesting Hb and Cs at electrode surface slowed down $[Fe(CN)_6]^{3-/4-}$ electron transfer. Drastic morphological changes occurred in SEM image (Fig.6A-B). Hb like a ball, was well dispersed and immobilized onto the surface of VA-ErGO-FF network, suggesting that the proposed biosensor has been successfully constructed.

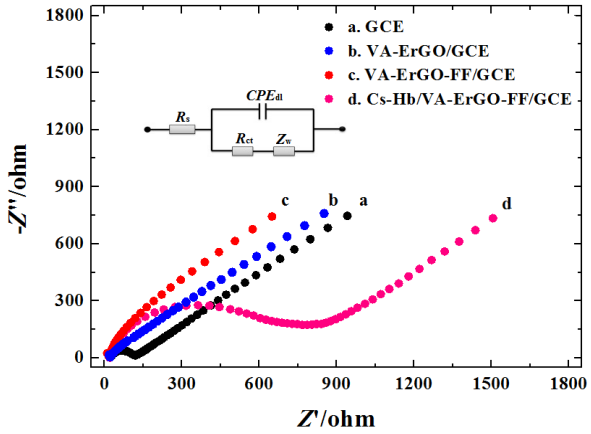

Figure 5. Bare GCE (curve a)'s electrochemical impedance spectroscopy (EIS), VA-ErGO/GCE (curve b), VA-ErGO-FF/GCE (curve c), Cs-Hb/VA-ErGO-FF/GCE (curve d) of 5.0×10^{-3} mol L^{-1} $[Fe(CN)_6]^{4-/3-}$ (1:1) solution with 0.10 mol L^{-1} KCl; open circuit potential and amplitude as 5 mV; scope of frequency in 100000 Hz - 0.01 Hz; inset illustrates equivalent circuit.

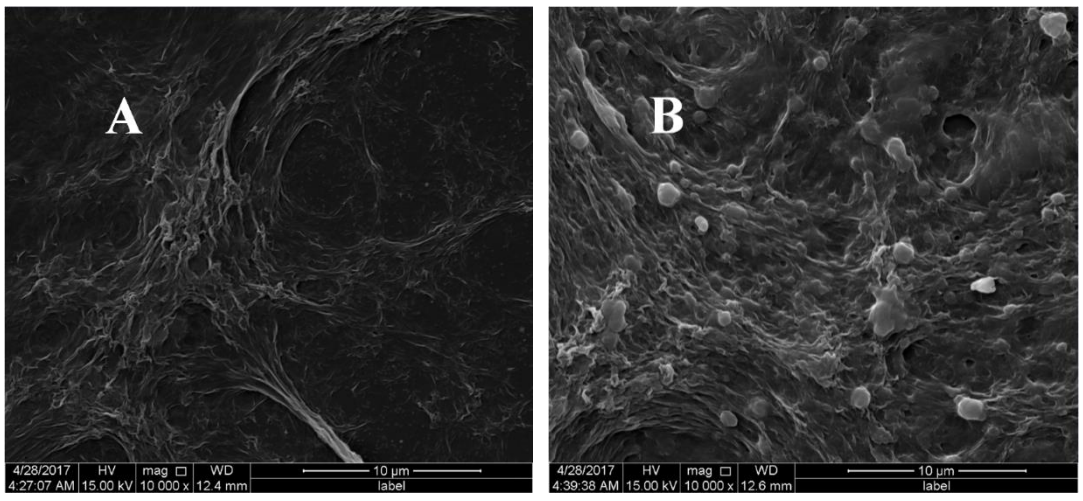

Figure 6. Typical top view SEM images retrieved by VA-ErGO-FF/GCE (A) and Cs-Hb/VA-ErGO-FF/GCE (B).

3.4. Direct electrochemistry of Cs-Hb/VA-ErGO-FF/GCE

Hb's direct electrochemical actions in VA-ErGO-FF network were investigated. Fig.7A shows the CVs of various modified electrodes of N_2-saturated 0.1 mol L^{-1} pH 7.0 PB solution. There was no obvious redox peak in VA-ErGO-FF/GCE, Cs/VA-ErGO-FF/GCE and Cs-Hb/GCE within observed potential scope. Two weak redox peaks were seen with E_{pc} as -0.385 V and E_{pa} as -0.290 V on Cs-Hb/VA-ErGO/GCE, proving features at Hb's heme $Fe^{(III)}/Fe^{(II)}$ redox peaks [42]. As proved by the results, the Hb-electrode surface DET may function via VA-ErGO in the role of conductive bridge. In the application of Cs-Hb/VA-ErGO-FF/GCE, redox response was reinforced to increase peak shape asymmetry (E_{pc} of -0.367 V and E_{pa} of -0.307 V), proving FF's facilitating effect on Hb's DET. Strongly reinforced peak currents and quite low ΔE_p exhibit a faster and efficient electron transfer process between modified electrode surface and active Hb site. Moreover, no changes in redox peak were found for consecutive 50 cycles, meaning the film's favorable stability after modification (Fig.7B). While in Cs-Hb/VA-ErGO/GCE, merely 89.47% initial peak currents were preserved after consecutive 50 cycles, which proved the bad stability of electrode devoid of FF. That was related to the synergy effect of these nanocomposites: FF may take directly Hb to entrance into VA-ErGO via π–π covalent bonding out of superb stability and biocompatibility, and VA-ErGO can offer massive surface area in layered structure to make up FF's poor conductivity.

CV was used to verify how scan rate affected Cs-Hb/VAErGO-FF/GCE's electrochemical responses (Fig.7C). According to Laviron[43], charge-transfer coefficient (α) should be 0.47, constant of Hb-modified electrode heterogeneous electron transfer rate (k_s) should be 1.89 s^{-1}. Meanwhile, equation $Q=nFA\Gamma^*$ [44] was employed for initial reporting. Hb's surface concentration (Γ^*) in biosensor of 8.17×10^{-10} mol cm^{-2} was 43 times greater compared with monolayer coverage (1.89×10^{-11} mol cm^{-2}) [45], which suggested multi-layer Hb's involvement under VA-ErGO-FF network during DET procedure. The abundant amount of electroactive protein molecule was partially due to VA-ErGO-FF network's good biocompatibility and benefited the loading of proteins.

Research was furthered to investigate how pH value affected Hb's electrochemical action in its range of 5.5 -8.0 (Fig.7D). pH value increase led to negative formal peak potential ($E^{0\prime}$) negative transfer. There was a favorable linear regression relation between $E^{0\prime}$ and pH, which could be computed by $E^{0\prime}$(V) = −0.0591 pH – 0.113 (R=0.998). Slope value was close to −59.0 mV pH^{-1} [46], meaning involvement of equal protons (H^+) and electrons (e^-) transfer amid electrode reaction.

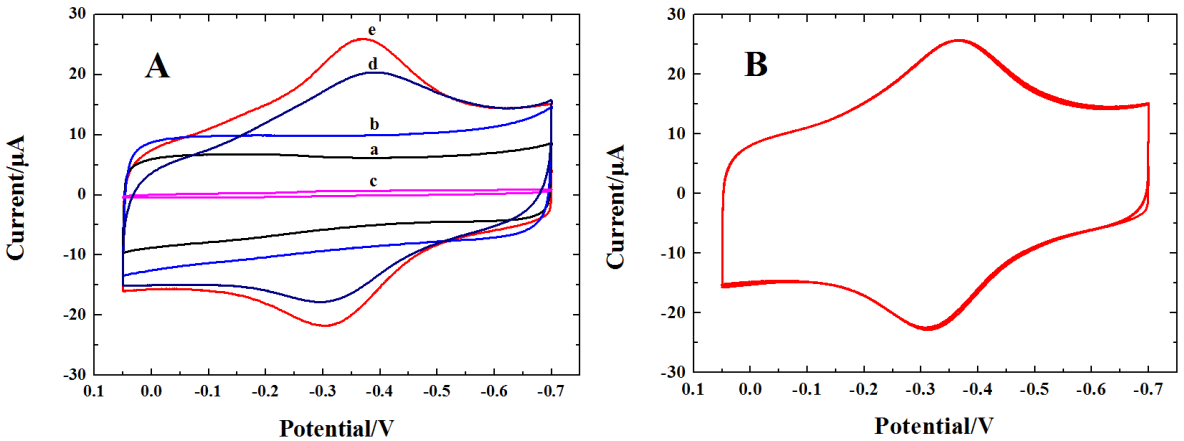

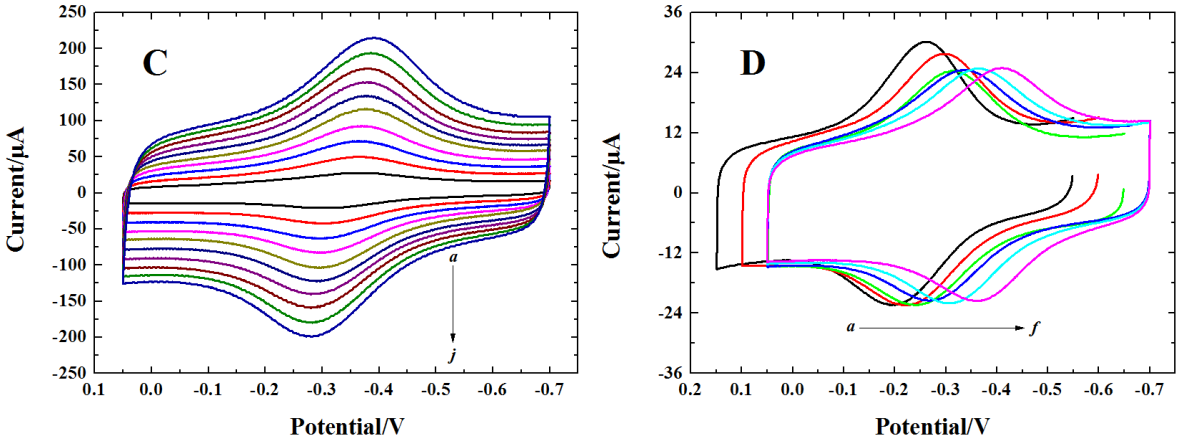

Figure 7. (A) CVs of VA-ErGO-FF/GCE (curve a), Cs/VA-ErGO-FF/GCE (curve b), Cs-Hb/GCE(curve c), Cs-Hb/ErGO/GCE (curve d) and Cs-Hb/VA-ErGO-FF/GCE (curve e) of N_2-saturated 0.1 mol L^{-1} pH 7.0 PB solutions, v=0.050 V s^{-1}; (B) Multi-scan CVs of Cs-Hb/VA-ErGO-FF/GCE of N_2-saturated 0.1 mol L^{-1} pH 7.0 PB solutions, v=0.050 V s^{-1}; (C) CVs of Cs-Hb/VA-ErGO-FF/GCE in N_2-saturated 0.1 mol L^{-1} pH 7.0 PB solutions at different scan rates; (D) CVs of Cs-Hb/VA-ErGO-FF/GCE in N_2-saturated 0.1 mol L^{-1} PB solutions with pH value as 5.5, 6.0, 6.5, 7.0, 7.5, 8.0 (*a–f*); v=0.050 V s^{-1}.

3.5. Electrocatalytic behavior of the biosensor to CH_3NO_2

To demonstrate the electrocatalytic activity of different electrodes to CH_3NO_2, CV was conducted and recorded. Fig.8A shows electrode CV of N_2-saturated 0.1 mol L^{-1} pH 7.0 PB solution with 2.0×10^{-4} mol L^{-1} CH_3NO_2. Among them, Cs-Hb/VA-ErGO-FF/GCE showed the best responses in catalyzing CH_3NO_2. This further confirmed Hb in the VA-ErGO-FF network are more active, and it can provide a more favorable environment for Hb than its pure component. Superb electrocatalytic activity may be attributable to two reasons. Firstly, for its high conductivity and biocompatibility, immobilized Hb molecule shows electrocatalytic activity to CH_3NO_2. Secondly, in its role of excellent support having favorable dispersity, VA-ErGO-FF network may add active sites and promote catalytic activity.

CH_3NO_2's amperometric response to various electrodes was observed. Fig.8B displayed electrode amperometric response I-t curve by 5.0×10^{-5} mol L^{-1} CH_3NO_2 successive addition into continuously stirred PB solutions with working potential as −0.80 V. Clearly, amperometric current underwent maximal growth upon successive addition of CH_3NO_2 was exhibited at Cs-Hb/VA-ErGO-FF/GCE, indicating that the VA-ErGO-FF network remarkably reinforced electrocatalytic activity. Aforementioned results reveal that Cs-Hb/VA-ErGO-FF/GCE may efficiently facilitate CH_3NO_2 reduction, which is feasible for the quantitative detection of CH_3NO_2.

Amperometric method was used for the establishment of sensitive assay frameworks. Biosensors generated steady-state amperometric responses to successive addition of CH_3NO_2 aliquot to PB solution with operating potential as −0.80 V (Fig. 8C). Fig.8D is the calibration chart of reduction current responses for CH_3NO_2. There was a favorable linear relation between response currents and CH_3NO_2 concentration in 1.0×10^{-6} -5.0×10^{-4} mol L^{-1}. Equation for regression: i_{pa} (μA) = 0.530 + 0.121c (μmol L^{-1}) (R=0.999). Predicted detection limit (S/N=3) was 5.0×10^{-7} mol L^{-1} CH_3NO_2 [47].

Moreover, calibration curve was gradually stabilized in case that CH_3NO_2 was continually accumulated in a way, demonstrating the representative properties in Michaelis–Menten kinetic system. Biosensor's apparent Michaelis–Menten constant (K_m^{app}) to CH_3NO_2 was computed as 0.57 mmol L^{-1} as per Lineweaver–Burk equation [48]. Low K_m^{app} value verified Hb's maintenance of bioelectrocatalytic activity in VA-ErGO-FF network and showed relatively high affinity to CH_3NO_2.

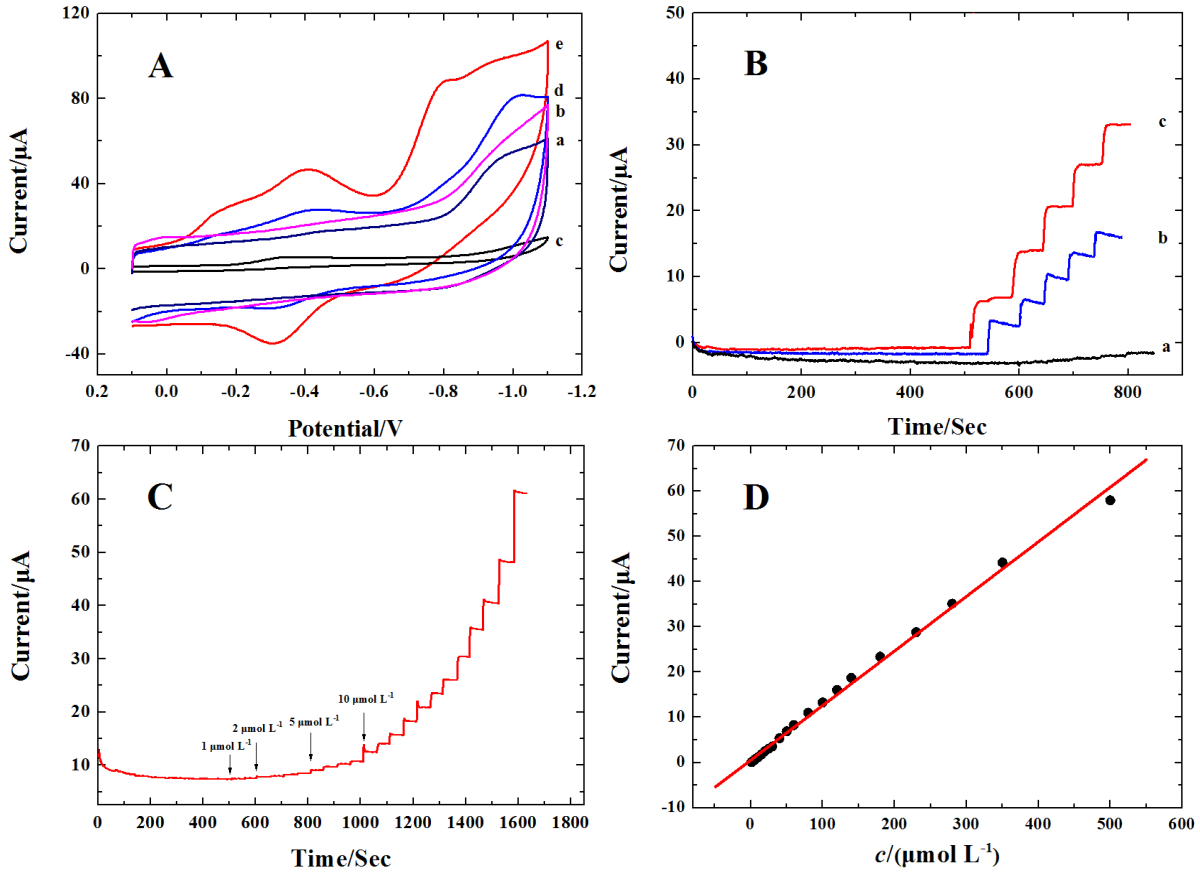

Figure 8. (A) CVs of VA-ErGO-FF/GCE (curve a), Cs/VA-ErGO-FF/GCE (curve b), Cs-Hb/GCE(curve c), Cs-Hb/ErGO/GCE (curve d) and Cs-Hb/VA-ErGO-FF/GCE (curve e) in N_2-saturated 0.1 mol L^{-1} pH 7.0 PB solutions containing 2.0×10^{-4} mol L^{-1} CH_3NO_2; (B) Amperometric responses of VA-ErGO-FF/GCE (curve a), Cs-Hb/ErGO/GCE (curve b), Cs-Hb/VA-ErGO-FF/GCE (curve c) of N_2-saturated 0.1 mol L^{-1} pH 7.0 PB solutions at −0.8 V with 5.0×10^{-5} mol L^{-1} CH_3NO_2 successive addition; (C) Cs-Hb/VA-ErGO-FF/GCE amperometric response in N_2-saturated 0.1 mol L^{-1} pH 7.0 PB solutions at -0.80 V to CH_3NO_2 successive addition; (D) corrected catalytic current curve against CH_3NO_2 concentrations.

Table 1 sums up the comparison for presented biosensor and other Hb-based CH_3NO_2 biosensors [18-21]. This presented biosensor showed excellent electrochemical properties. In contrast to G-Cs/Hb/G/IL/GCE [18], Hb/IL/MWCNTs/GCE [19], Cs-Hb/3DG-NCNTs/GCE [21], it has much broader linear scope. In contrast to Hb-Cs/GO-Cs/GCE [20], its detection limit is relatively lower.

Table 1. Contrast for electrochemical CH_3NO_2 biosensor performance.

Hb modified electrodes	k_s (s^{-1})	Γ* (mol cm^{-2})	Linear range (μmol L^{-1})	Detection limit (μmol L^{-1})	Ref.
G-Cs/Hb/G/IL/GCE	57.3	7.70×10^{-10}	0.0020−0.2300	0.0006	[18]
Hb/IL/MWCNTs/GCE	29.51	6.53×10^{-10}	0.0447−4.45	0.0134	[19]
Hb-Cs/GO-Cs/GCE	6.48	8.00×10^{-10}	5.0−1460.0	1.5	[20]
Cs-Hb/3DG-NCNTs/GCE	7.12	8.67×10^{-10}	0.5−350.0	0.15	[21]
Cs-Hb/VAErGO-FF/GCE	1.89	8.17×10^{-10}	1.0−500.0	0.5	This work

3.6. Reproducibility, stability and selectivity of the biosensor

Presented CH_3NO_2 biosensor was measured in reproducibility and stability. Measurement for 1.0×10^{-4} mol L^{-1} CH_3NO_2 concentrations had been repeated in 5 cycles (Fig.9A), with standard deviation (RSD) as 3.7%, proving the biosensor's good repeatability. Besides, these five separate sensors' RSD as 4.4% proved superb reproducibility in sensor preparation and electrode material's fine stability. After being stored for 15 days, current response was reduced by 7.4%, suggesting the extraordinary stability of biosensor.

Selectivity means a lot to the real application of electrochemical biosensor. Biosensor selectivity was measured with amperometric current-time approach, interfering substance HPO_4^-, C_6H_{14}, NO_2^-, NO_3^- included. The observed results (Fig.9B) clearly indicated that above observed substances had no obvious interference for presented biosensor, verifying the high selectivity of biosensor.

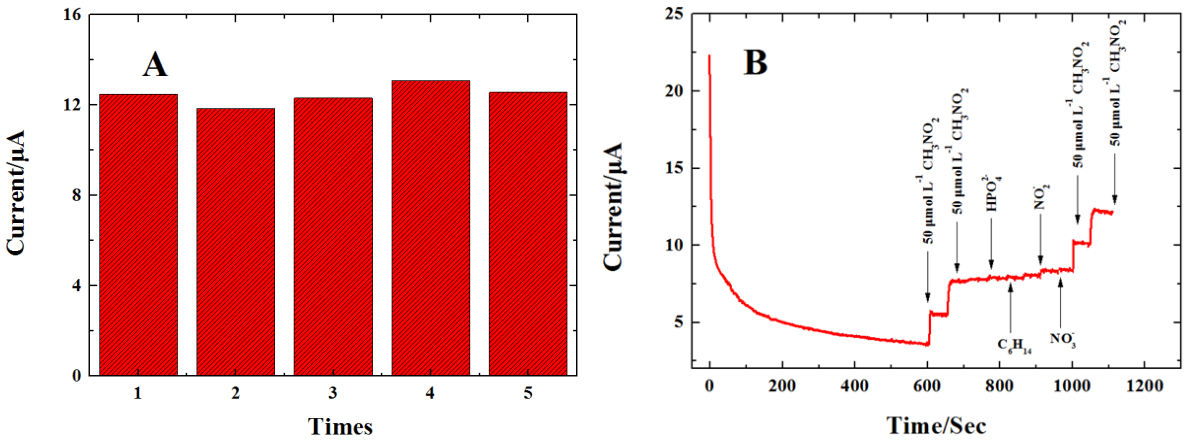

Figure 9. (A) Sensor amperometric response to five individual determination of 1.0×10^{-4} mol L^{-1} CH_3NO_2; (B) Five sensors' amperometric response in 1.0×10^{-4} mol L^{-1} CH_3NO_2.

3.7. Practical applications of the biosensor

Presented biosensor's practicability was verified through lake water samples' CH_3NO_2 determination. For low CH_3NO_2 concentration of sample, presented biosensor could not be applied. Therefore, recovery test was carried out with standard addition. Recovery and RSD value summarized

in Table 2 verify the feasibility of applying presented biosensor in sample CH_3NO_2 analysis.

Table 2. Presented biosensor's recovery results to CH_3NO_2 determination for lake water samples (n = 3).

Samples	CH_3NO_2 concentration (μmol L^{-1})		Recovery (%)	RSD (%)
	Added	Found		
1	1.00	1.02±0.07	102.0	2.7
2	25.00	25.04±0.61	100.2	3.4
3	50.00	49.17±1.01	98.34	4.2
4	100.00	97.98±2.78	97.98	3.9

4. CONCLUSIONS

In this paper, the VA-ErGO-FF network on GC electrode surface was prepared directly from GO-FF dispersions by using PPM. Such a VA-ErGO-FF network gained further application in the immobilization of model molecule Hb to construct an electrochemical CH_3NO_2 biosensor. Because of GO's excellent electrical performance and Hb's biocompatibility, immobilized Hb molecule had reinforced electron transfer rate on dual redox peaks, indicating the capacity of VA-ErGO-FF network to offer a good environment to Hb. Moreover, the fabricated biosensor enjoyed fine electrocatalytic responses to CH_3NO_2 reduction. Thus, VA-ErGO-FF network can be an ideal electrochemical sensing platform of application in electrochemical biosensors.

ACKNOWLEDGEMENTS
The authors gratefully acknowledge the financial supported by the Program for Science and Technology Innovative Research Team in Higher Educational Institutions of Henan Province (No.20IRTSTHN008), and the National Natural Science Foundation of China (No. 21572046). Financial support from the Cultivation Foundation of Henan University of Engineering (PYXM202009) is gratefully acknowledged.

References

1. S. Singh, *J. Hazard. Mater.*, 144 (2007) 15.
2. E. H. Page, A. K. Pajeau, T. C. Arnold, A. R. Fincher, M. J. Goddard, *Am. J. Ind. Med.*, 40 (2001) 107.
3. L. R. Jones, J. A. Riddick, *Anal. Chem.*, 28 (1956) 1493.
4. K. U. Alwis, B. C. Blount, L. K. Silva, M. M. Smith, K. H. Loose, *Environ. Sci. Technol.*, 42 (2008) 2522.
5. R. L. Martins, C. D. Veloso, C. A. Mota, M. Schmal, *J. Mol. Catal. A-Chem.*, 330 (2010) 88.

6. M. S. Meaney, V. L. McGuffin, *Anal. Chim. Acta*, 610 (2008) 57.
7. H. Liu, K. Guo, C. Y. Duan, X. N. Dong, J. J. Gao, *Biosens. Bioelectron.*, 87 (2017) 473.
8. X. Q. Liu, R. Yan, J. M. Zhang, J. Zhu, D. K. Y. Wong, *Biosens. Bioelectron.*, 66 (2015) 208.
9. S. Lopez-Bernabeu, A. Gamero-Quijano, F. Huerta, E. Morallon, F. Montilla, *J. Electroanal. Chem.*, 793 (2017) 34.
10. F. W. Scheller, N. Bistolas, S. Q. Liu, M. Janchen, M. Katterle, U. Wollenberger, *Adv. Colloid Interface Sci.*, 116 (2005) 111.
11. T. R. Zhan, X. J. Wang, Y. M. Zhang, Y. Song, X. L. Liu, J. Xu, W. G. Hou, *Sensor. Actuat. B-Chem.*, 220 (2015) 1232.
12. Y. J. Wu, F. Wang, K. Lu, M. X. Lv, Y. F. Zhao, *Sensor. Actuat. B-Chem.*, 244 (2017) 1022.
13. T. R. Zhan, Z. W. Tan, X. J. Wang, W. G. Hou, *Sensor. Actuat. B-Chem.*, 255 (2018) 149.
14. Q. Lu, C. Hu, R. Cui, S. Hu, *J. Phys. Chem. B*, 111 (2007) 9808.
15. S. Zhang, D. W. Zhang, Q. L. Sheng, J. B. Zheng, *J. Solid State Electrochem.*, 18 (2014) 2193.
16. W. S. Zhao, X. Y. Li, Z. R. Wen, X. L. Niu, Q. F. Shen, Z. L. Sun, R. X. Dong, W. Sun, *Int. J. Electrochem. Sci.*, 12 (2017) 4025.
17. W. Chen, X. L. Niu, X. Y. Li, X. B. Li, G. J. Li, B. L. He, Q. T. Li, W. Sun, *Mat. Sci. Eng. C-Mater.*, 80 (2017) 135.
18. L. Wang, X. Zhang, H. Xiong, S. Wang, *Biosens. Bioelectron.*, 26 (2010) 991.
19. Y. M. Wang, H. Y. Xiong, X. H. Zhang, Y. Ye, S. F. Wang, *J. Electroanal. Chem.*, 674 (2012) 17.
20. Y. Wen, W. Wen, X. Zhang, S. Wang, *Biosens. Bioelectron.*, 79 (2016) 894.
21. F. Wang, Y. J. Wu, X. T. Sun, L. Z. Wang, K. Lu, *J. Electroanal. Chem.*, 824 (2018) 83.
22. A. K. Geim, *Science*, 324 (2009) 1530.
23. A. K. Geim, K. S. Novoselov, *Nat. Mater.*, 6 (2007) 183.
24. Y. Y. Shao, J. Wang, H. Wu, J. Liu, I. A. Aksay, Y. H. Lin, *Electroanalysis*, 22 (2010) 1027.
25. J. H. Fang, I. Levchenko, S. Kumar, D. H. Seo, K. Ostrikov, *Sci. Technol. Adv. Mat.*, 15 (2014)
26. X. J. Fan, Z. W. Peng, R. Q. Ye, H. Q. Zhou, X. Guo, *ACS Nano*, 9 (2015) 7407.
27. J. X. Yan, Y. C. Leng, Y. N. Guo, G. Q. Wang, H. Gong, P. Z. Guo, P. H. Tan, Y. Z. Long, X. L. Liu, W. P. Han, *ACS Appl. Mater. Inter.*, 11 (2019) 10810.
28. H. L. Guo, X. F. Wang, Q. Y. Qian, F. B. Wang, X. H. Xia, *ACS Nano*, 3 (2009) 2653.
29. Y. Shao, J. Wang, M. Engelhard, C. Wang, Y. Lin, *J. Mater. Chem.*, 20 (2010) 743.
30. J. F. Ping, Y. X. Wang, K. Fan, J. Wu, Y. B. Ying, *Biosens. Bioelectron.*, 28 (2011) 204.
31. Z. J. Wang, X. Z. Zhou, J. Zhang, F. Boey, H. Zhang, *J. Phys. Chem. C*, 113 (2009) 14071.
32. J. F. Ping, Y. X. Wang, Y. B. Ying, J. Wu, *Anal. Chem.*, 84 (2012) 3473.
33. M. A. Raj, S. A. John, *J. Phys. Chem. C*, 117 (2013) 4326.
34. Q. Zhang, Y. Qiao, F. Hao, L. Zhang, S. Wu, Y. Li, J. Li, X. M. Song, *Chem.-Eur. J.*, 16 (2010) 8133.
35. Q. Zhang, S. Wu, L. Zhang, J. Lu, F. Verproot, Y. Liu, Z. Xing, J. Li, X. M. Song, *Biosens. Bioelectron.*, 26 (2011) 2632.
36. Y. Gong, X. Chen, Y. Lu, W. Yang, *Biosens. Bioelectron.*, 66 (2015) 392.
37. K. Liu, J. Zhang, G. Yang, C. Wang, J. J. Zhu, *Electrochem. Commun.*, 12 (2010) 402.
38. W. S. Hummers, R. E. Offeman, *J. Am. Chem. Soc.*, 80 (1958) 1339.
39. H. B. Wang, Q. Zhang, X. Chu, T. T. Chen, J. Ge, R. Q. Yu, *Angew. Chem. Int. Edit.*, 50 (2011) 7065.
40. F. Wang, K. Ding, C. Zhang, W. K. Jia, K. Lu, Y. J. Ye, *J. Electrochem. Soc.*, 164 (2017) H1033.
41. Y. Wu, A. Zhou, H. Yang, F. Wang, K. Lu, *Materials*, 11 (2018) 322.
42. L. Wang, W. Qi, R. Su, Z. He, *J. Solid State Electrochem.*, 17 (2013) 2595.
43. E. Laviron, *J. Electroanal. Chem.*, 101 (1979) 19.
44. S. Palanisamy, C. Karuppiah, S. M. Chen, R. Emmanuel, P. Muthukrishnan, P. Prakash, *Sensor. Actuat. B-Chem.*, 202 (2014) 177.
45. S. F. Wang, T. Chen, Z. L. Zhang, X. C. Shen, Z. X. Lu, D. W. Pang, K. Y. Wong, *Langmuir*, 21

(2005) 9260.
46. R. S. Nicholson, *Anal. Chem.*, 37 (1965) 1351.
47. J. N. Miller, J. C. Miller, Statistics and Chemometrics for Analytical Chemistry, fourth ed., Pearson Education Limited, London, 2000
48. R. A. Kamin, G. S. Wilson, *Anal. Chem.* 52 (1980) 1198.